J Sol-Gel Sci Techn (2006) 39:285–291
DOI 10.1007/s10971-006-7780-5

# Characterization and application of $Fe_3O_4/SiO_2$ nanocomposites

**G.H. Du · Z.L. Liu · X. Xia · Q. Chu · S.M. Zhang**

Received: 9 November 2005 / Accepted: 16 February 2006 / Published online: 27 June 2006


**Abstract** A sol-gel procedure was used to cover $Fe_3O_4$ nanoparticles with $SiO_2$ shell, forming a core/shell structure. The core/shell nanocomposites were synthesized by a two-step process. First, $Fe_3O_4$ nanoparticles were obtained through co-precipitation and dispersed in aqueous solution through electrostatic interactions in the presence of tetramethylammonium hydroxide (TMAOH). In the second step, $Fe_3O_4$ was capped with $SiO_2$ generated from the hydrolyzation of tetraethyl orthosilicate (TEOS). The structure and properties of the formed $Fe_3O_4/SiO_2$ nanocomposites were characterized and the results indicate that the $Fe_3O_4/SiO_2$ nanocomposites are superparamagnetic and are about 30 nm in size. Bioconjugation to IgG was also studied. Finally, the mechanism of depositing $SiO_2$ on magnetic nanoparticles was discussed.

**Keywords** Sol-gel method · $Fe_3O_4/SiO_2$ nanocomposites · Superparamagnetic · Application in biomedical field

## 1. Introduction

Nanoscale magnetic materials have attracted considerable attention in recent years because of their potential applications in information storage, magnetic refrigeration, magneto-optical solid devices, cell separation and magnetic resonance imaging enhancement [1–6], etc. Many of these applications require magnetic nanoparticles embedded in a nonmagnetic matrix [7–10]. Applications in medical realm have increased the interests of encapsulating magnetic nanoparticles into silica. The nontoxic silica is an ideal coating material because of its capability to form extensive cross-linking, which leads to an inert outer shield. Silanized nanocomposites are stable in a wide range of biological environments, including physiological and supraphysiological salt concentrations. They are biocompatible and can also be easily activated to provide new functional group.

In the past few decades, many methods have been developed for coating silica on magnetic nanoparticles, including sol-gel [10], aerosol pyrolysis [11], micelle microemulaion [12], etc [13]. Most of these methods adopt a one-pot routine to form magnetic nanoparticles and silica coating simultaneously, which often results in magnetic cores with poor quality due to the coexistence of multiple iron oxide phases. On the other hand, it is relatively easy to control the properties of the magnetic naoparticles if they were prepared in a separate step prior to coating. Several groups have synthesized magnetic nanoparticles with desirable properties with coated organic molecule, then directly grew silica shell on their surfaces [14]. For example, spindle-type hematite magnetic nanoparticles with several hundred nanometers in size have been successfully capped with silica utilizing the hydrolysis of TEOS [15, 16]. Furthermore, Silicate has been used to form silica on iron oxide in aqueous solution stablized by tetramethylammonium hydroxide (TMAOH).

In this study, we present a method in which magnetic $Fe_3O_4$ nanoparticles were prepared using conventional co-precipitation process and dispersed in aqueous solution based on electrostatic repulsive interaction. Upon addition of precursors, silica coating would grow directly on the surface

G. Du (✉) · Z. Liu · X. Xia
Department of Physics, Huazhong University of Science and Technology (HUST), Wuhan, 430074, China
e-mail: guihuan_du@163.com

Z. Liu
e-mail: zlliu@hust.edu.cn

Q. Chu · S. Zhang
Tongji Hospital, Huazhong University of Science and Technology (HUST), Wuhan, 430070, China

of $Fe_3O_4$. Transmission Electron Microscopy (TEM), X-ray Photoelectron Spectroscopy (XPS), Fourier Transform Infrared Spectrometer (FTIR), Vibrating Sample Magnetometer (VSM), and Thermogravimetric Analysis (TGA) were used to characterize the $Fe_3O_4/SiO_2$ nanocomposites and revealed that the nanocomposites were about 30 nm in size with superparamagnetic behavior. Mechanism of depositing $SiO_2$ on magnetic nanoparticles was discussed. Finally, the nanocomposites were tested for their bioconjugation ability with two types of antibody.

## 2. Experimental

### 2.1. Synthesis of $Fe_3O_4$ nanoparticles

$Fe_3O_4$ nanoparticles were synthesized by using a co-precipitation process [9]. Briefly, $FeCl_3 \cdot 6H_2O$ and $FeCl_2 \cdot 4H_2O$ (2:1 molar ratio) were loaded into a three-neck flask and dissolved in 100 ml Millipore water. Ammonia hydroxide was then added drop-wise into the vigorously stirred solution at 40°C. After ammonia ran out, an additional 15 min was required to form stable nanoparticles. Then the $Fe_3O_4$ nanoparticles were collected by permanent magnetic field and washed with water to remove unreacted ammonia. Tetramethylammonium hydroxide (TMAOH) solution (25 wt% in water) was added into the collected $Fe_3O_4$ and stirred for 30 min to form stable colloid. Nitrogen was used in the whole process to prevent the particles from oxidation.

### 2.2. Synthesis of $Fe_3O_4/SiO_2$ nanocomposites

The $Fe_3O_4/SiO_2$ nanocomposites were prepared by adding tetraethyl orthosilicate (TEOS) into a mixture of ammonium hydroxide and TMAOH dispersed $Fe_3O_4$ in water-ethanol (1 + 10) solution. Typically, 1 g of $Fe_3O_4$ nanoparticles dispersed in TMAOH and 6 ml ammonium hydroxide was added to 50 ml water-ethanol (1 + 10) solution. TEOS solution (1 ml of TEOS in 49 ml of anhydrous ethanol) was added in a drop wise manner into the vigorously stirred solution. The mixture became gelatinized gradually because of the hydrolysis of TEOS. The gelatin was then kept for another 24 h to ensure maximum hydrolysis. Finally, it was dried under vacuum at 110°C for 2 days. The dried powder was ready for the following characterization.

### 2.3. Characterization

The structure and properties of the $Fe_3O_4/SiO_2$ nanocomposite samples were characterized by TEM, XPS, FTIR, VSM, and TGA. TEM was performed on a JEM—100CXIITransmission Electron Microscope with an acceleration voltage of 80 kV. Samples for TEM were prepared by redispersing the nanocomposite in ethanol and then applied drop-wise onto copper grids. Dried samples were submitted to ESCA 3600 Shimadzu X-ray Photoelectron Spectroscopy directly for surface analysis. For FTIR, nanocomposites were mixed with KBr and pressed into tablets and the spectrum were obtained on a Bluker EQUINOX 55 Fourier Transform Infrared Spectrometer. Magnetization curves were measured at room temperature using a TM-VSM2050HGC Vibrating Sample Magnetometer. TGA was carried out with a heating rate of 10°C/min using a Netzsch STA 409 + Bluker EQUINOX 55 Thermal Analysis—Fourier Transform Infrared Thermogravimetric Analyzer in air with a temperature of up to 800°C. The stability of $Fe_3O_4/SiO_2$ nanocomposite was evaluated by measuring the concentration of $Fe^{2+}$ ion from samples dispersed in acidic or basic solutions. The concentration of $Fe^{2+}$ was recorded on a Perkin-Elmer AA300 Atom Absorb Spectrophotometer to evaluate the stability of the powders in acidic or basic solution.

## 3. Results and discussion

### 3.1. Preparation of $Fe_3O_4/SiO_2$ nanocomposites

The procedure and condition described in the experimental section are optimized for the preparation of $Fe_3O_4/SiO_2$ nanocomposites. To decide a suitable condition for the synthesis, we compared the morphology and the magnetic properties of samples made under different conditions. In the process of synthesizing $Fe_3O_4/SiO_2$, the ratio between ammonia and ethanol was found to be an important parameter, since it determines the velocity of particle growth.

Figure 1 shows TEM micrographs of several samples prepared at different ammonia to ethanol ratios. The hydrolysis velocity of TEOS may be a main factor that determines the size of the final particles. The hydrolysis can be catalyzed by acid or base (in this case ammonia is used to provide the $OH^-$). At high ammonia to ethanol ratios, the amount of $OH^-$ was in excess. That could induce fast hydrolysis of TEOS and the networks of Si–O band were connected to each other to form bigger particles. On the contrary, insufficient $OH^-$ leads to slow hydrolysis where most TEOS would not hydrolyze on the surface of $Fe_3O_4$. Instead, it would cause nucleation of $SiO_2$ and result in small $Fe_3O_4/SiO_2$ nanocomposites.

Figure 2 gives the broad and narrow scan XPS spectra of $Fe_3O_4$ nanoparticles and $Fe_3O_4/SiO_2$ nanocomposites. For $Fe_3O_4$, the peaks at 711.0 eV and 724.0 eV are the characteristic doublets of Fe $2P_{3/2}$ and Fe $2P_{1/2}$ from iron oxide. The data is consistent with the reported values of $Fe_3O_4$ in the literature [17]. No peak for Fe is observed in curve of $Fe_3O_4/SiO_2$ nanocomposites. The peaks at 103.6 eV and 533.2 eV are assigned to Si 2p and O 1s. This indicates that $SiO_2$ is deposited on the $Fe_3O_4$ surface, forming a core/shell structure.

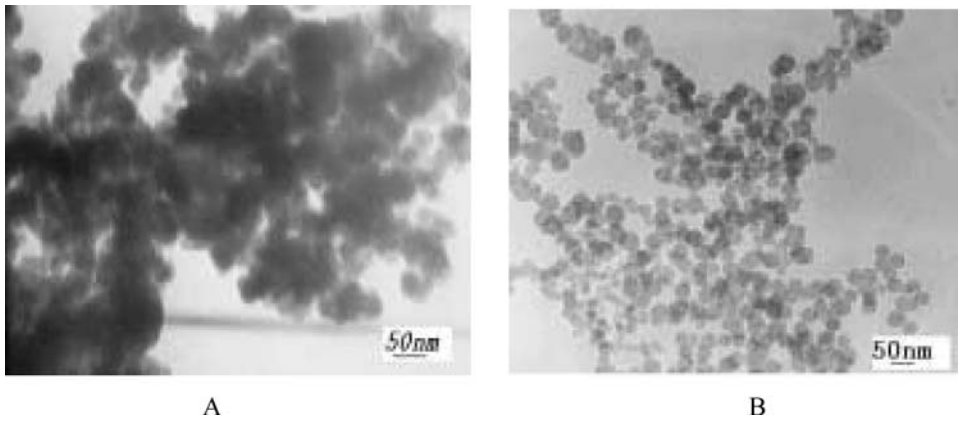


**Fig. 1** TEM images of $Fe_3O_4/SiO_2$ nanocomposites with deferent ratios of ammonia to ethanol. The ratio is 1:5 for A, and 1:10 for B

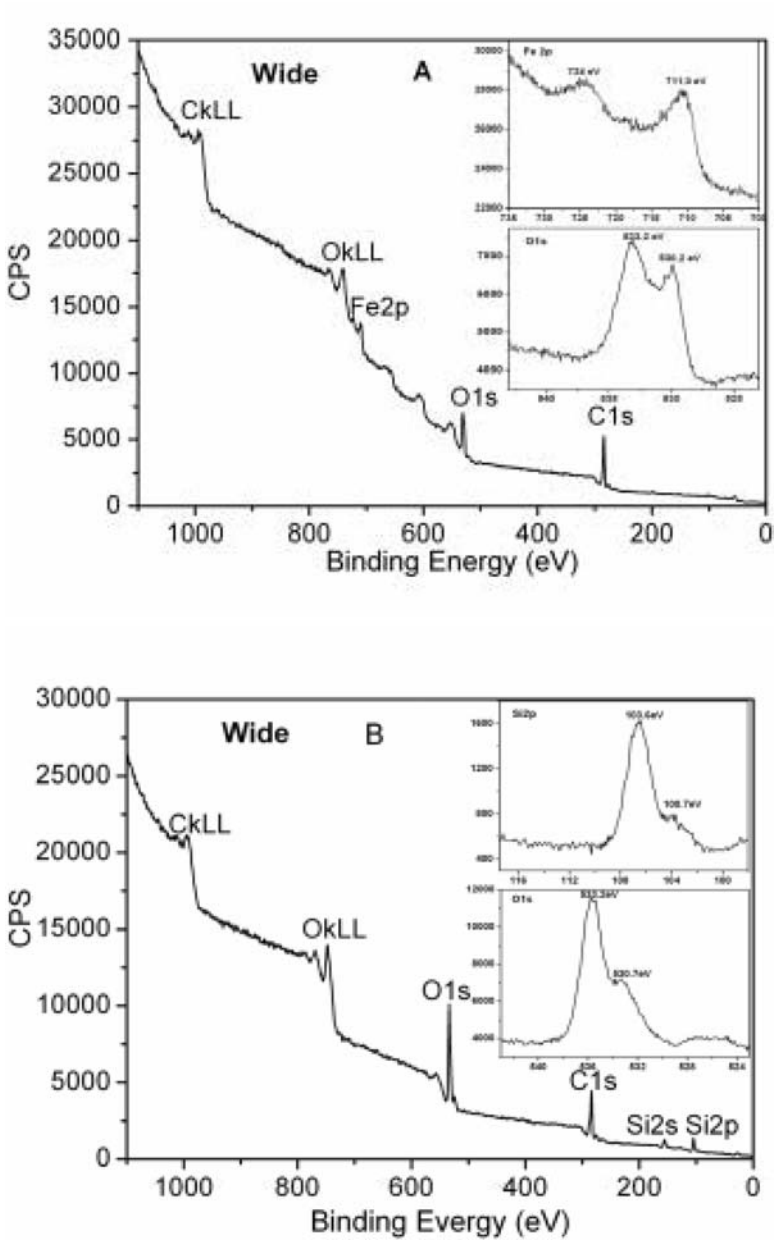


**Fig. 2** XPS broad scan spectra of $Fe_3O_4$ nanoparticles (A) and $Fe_3O_4/SiO_2$ nanocomposites (B). The insets are narrow scan for Fe 2p, O 1s and Si 2p, O 1s, respectively

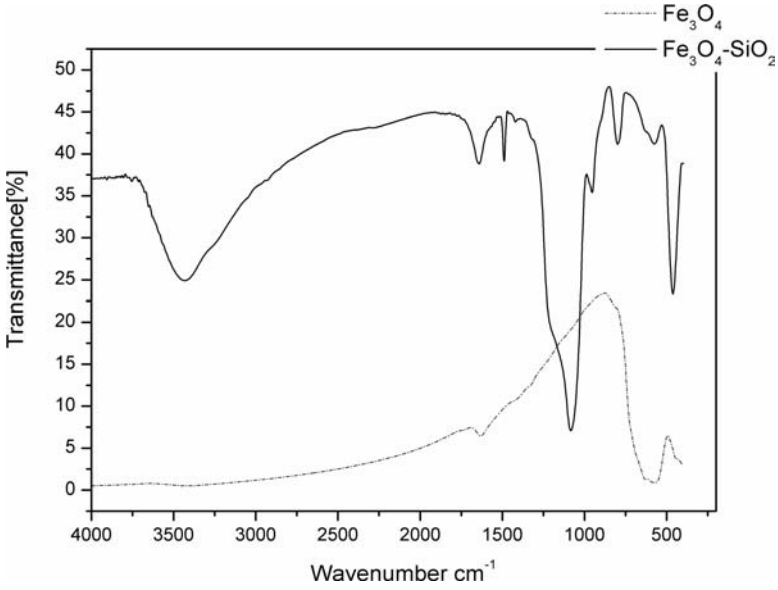


**Fig. 3** FTIR spectra of $Fe_3O_4$ and $Fe_3O_4/SiO_2$ nanoparticles

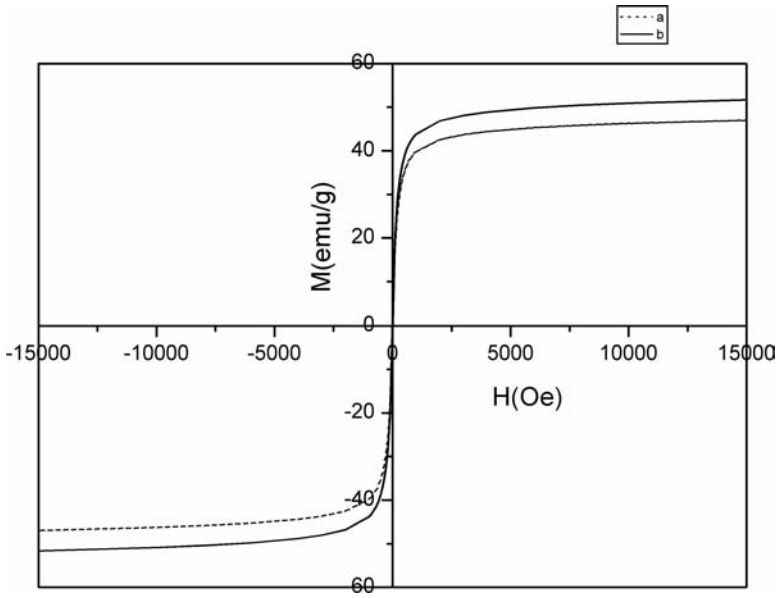


**Fig. 4** Magnetization of the (a) $Fe_3O_4$ nanoparticles and (b) $Fe_3O_4/SiO_2$ nanocomposites

### 3.2. FTIR Spectra

Figure 3 shows the FTIR spectra of the $Fe_3O_4$ and $Fe_3O_4/SiO_2$. In the case of $Fe_3O_4/SiO_2$ (solid line), the broad bands centered around 3428 and 1640 $cm^{-1}$ are assigned to the H–O–H stretching modes and bending vibration of the free or adsorbed water, respectively. The characteristic absorption for the silica network is assigned as follows. The broad high-intensity band at 1080 $cm^{-1}$ is due to the asymmetric stretching bonds of Si–O–Si in $SiO_4$ tetrahedron associated with the motion of oxygen in Si–O–Si antisymmetrical stretch. The band at 798 $cm^{-1}$ is assigned to the Si–O–Si symmetric stretch, while the sharp band at 461 $cm^{-1}$ corresponds to the Si–O–Si or O–Si–O bending mode. The band at 574 $cm^{-1}$ is an indication of the presence of Si–O–Fe. In the $Fe_3O_4$ curve, three main absorptions centered around 582, 1630 and 3380 $cm^{-1}$ were observed, each corresponding to Fe–O, O–H bending vibration and O–H stretching vibration, respectively. Based on this information, we conclude that $Fe_3O_4$ is covered by $SiO_2$ layer that exhibits its characteristic IR vibration bands.

### 3.3. Magnetic properties of $Fe_3O_4/SiO_2$ nanocomposites

The occurrence of superparamagnetism for $Fe_3O_4$ nanoparticles and $Fe_3O_4/SiO_2$ nanocomposites was confirmed by the closed *M-H* loops shown in Fig. 4. No reduced remanence

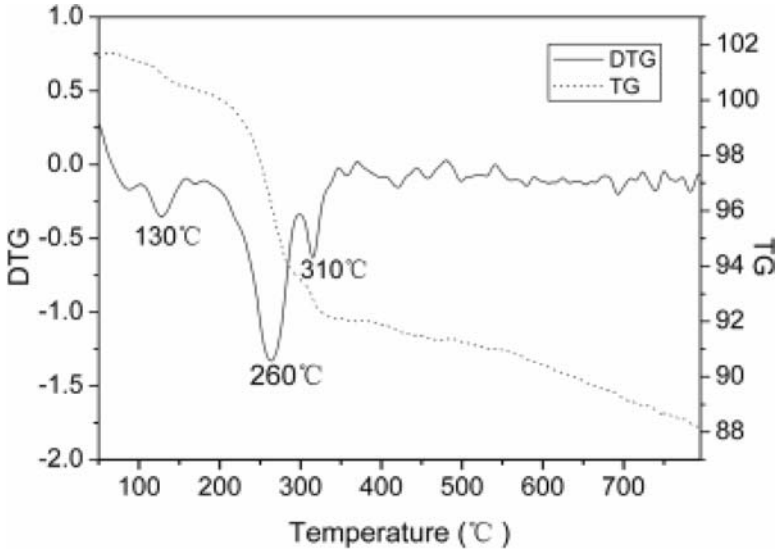


**Fig. 5** TG and DTG curves of $SiO_2/Fe_3O_4$ nanocomposites

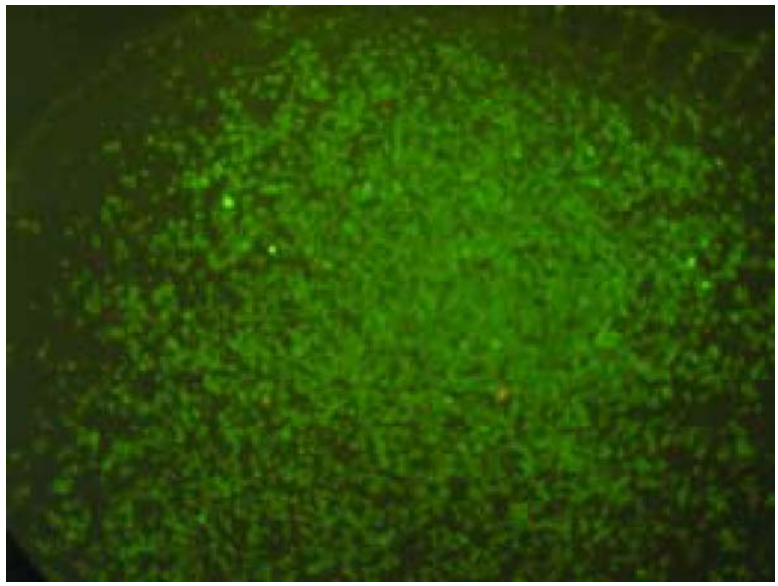

**Fig. 6** The Fluorescence microscope image of nanocomposites linking to FITC-antibody

and coercivity were observed in curves a and b. The saturation magnetization (Ms) of $Fe_3O_4/SiO_2$ and the $Fe_3O_4$ nanoparticles are 44.5 emu/g and 51.2 emu/g, respectively. The decline difference in Ms can be ascribed to the deposition of nonmagnetic $SiO_2$ on $Fe_3O_4$. Assuming only the amount of $SiO_2$ influences magnetization, the content of $SiO_2$ is about 13 wt%.

### 3.4. Stability tests of $Fe_3O_4/SiO_2$ nanocomposites

The stability of the $Fe_3O_4/SiO_2$ nanocomposite was studied by measuring its integrity under heat and acid corrosion. The protection of silica shell was studied by dispersing the $Fe_3O_4/SiO_2$ nanocomposites in 0.1 mol/L HCl or 0.1 mol/L NaOH solution for 20 hrs. The solutions were then centrifuged and supernatants were collected to measure the presence of $Fe^{2+}$. The concentration of $Fe^{2+}$ was measured by Atomic Absorption Spectrophotometer. In this experiment, no $Fe^{2+}$ was found in the solution, indicating $SiO_2$ shell has good protection ability.

The heat endurance of $Fe_3O_4/SiO_2$ nanocomposites was tested by thermo-gravimetric (TG). TG and differential thermo-gravimetric (DTG) curves are shown in Fig. 5. The curve exhibits three distinct weight loss stages. The small weight loss at lower temperature of about 130°C is probably due to the evaporation of residual alcohol and physically adsorbed water. The two weight losses at about 260°C and 310°C come from the decomposition of organic substances in $SiO_2/Fe_3O_4$ nanocomposites. There is little weight loss between 330–800°C, indicating that the $Fe_3O_4/SiO_2$ nanocomposites are stable up to 800°C.

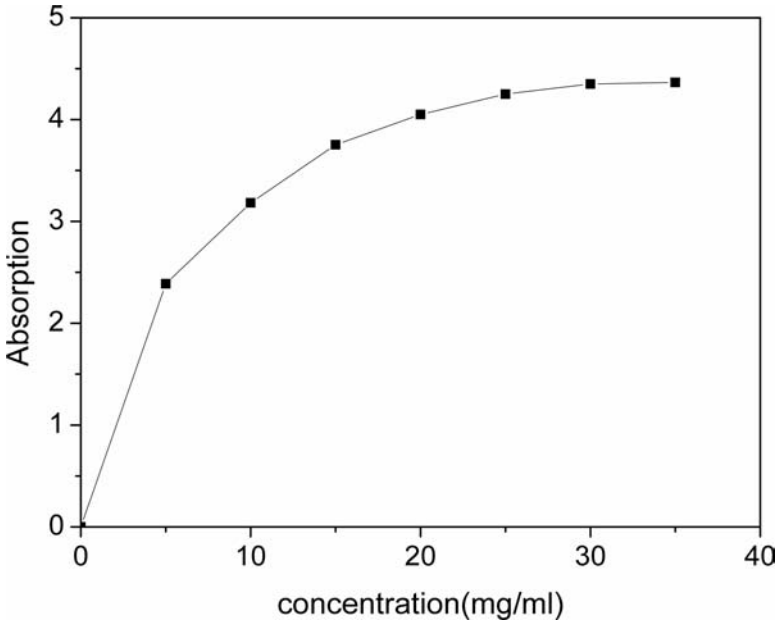


**Fig. 7** The relationship between absorption and the concentration of the $SiO_2/Fe_3O_4$ nanocomposites aqueous solution

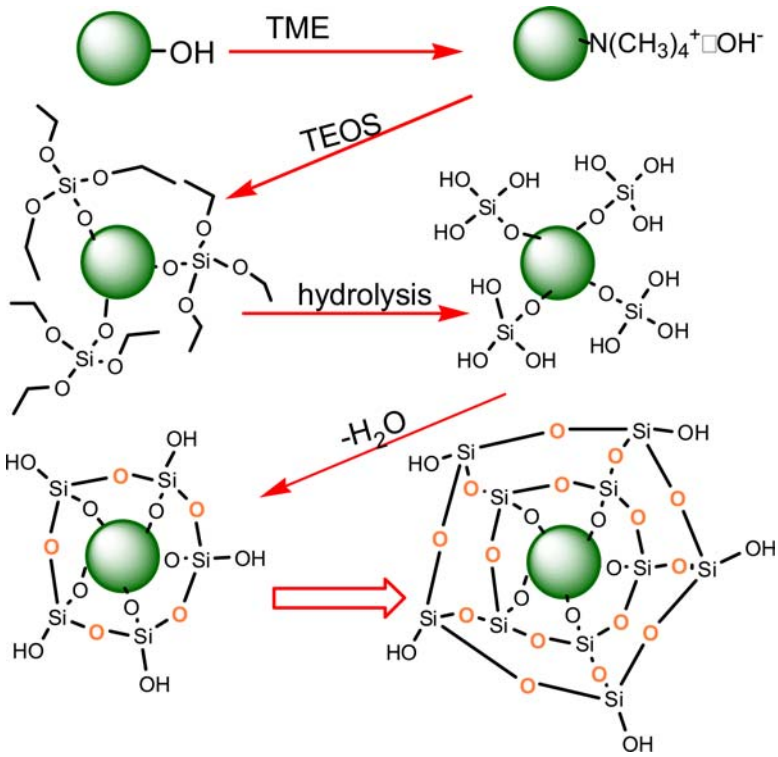


**Fig. 8** General procedures for coating silica

### 3.5. Conjugating $SiO_2/Fe_3O_4$ nanocomposites to biomolecule

Bioconjugation was tested by covalently linking $Fe_3O_4$ nanocomposite to FITC-labeled antibody. $SiO_2/Fe_3O_4$ nanocomposites were activated with N-hydroxysuccinimide ester (NHS) and 1-ethyl-3-(3-dimethylaminopropyl) carbodiimide (EDC), before mixing with FITC-labeled antibody at ambient temperature for 30 min. Solvent containing unlabeled antibody was decanted by collecting nanocomposites with magnets and washing them for several times with PBS solution. Fluorescence micrograph of the biomolecule decorated nanocomposites is shown in Fig. 6, from which we can see the $SiO_2/Fe_3O_4$ nanocomposites have good ability to link to biomolecule.

Antibody from the reagent kit HCG SEROZYME, which diagnoses pregnancy before the next catamenia was also used to test the ability of $SiO_2/Fe_3O_4$ nanocomposites conjugating to biomolecule. The antibody was blocked with bovine serum albumin in PBS solution to eliminate nonspecific binding. The absorption at 550 nm demonstrates the formation of the antibody-nanoparticle conjugates. Fig. 7 presents the absorption at different concentration of $SiO_2/Fe_3O_4$ nanocomposites. The absorption increases gradually as the increase of the concentration of the $SiO_2/Fe_3O_4$ nanocomposites and reached maximum at about 25 mg/ml.

### 3.6. Mechanisms of $Fe_3O_4/SiO_2$ nanocomposites formation

The process of synthesizing $Fe_3O_4/SiO_2$ particles includes the preparation of $Fe_3O_4$ nanoparticles and the deposition of $SiO_2$. Fig. 8 shows the general procedure of adsorbing course of TMAOH and the formation of $Fe_3O_4/SiO_2$ composites. First TMAOH is adsorbed onto the particles at pH above 12. Interactions between $N(CH_3)_4^+$ counterions and adsorbed $OH^-$ prevent the particles from aggregation and making the solution stable. In ferrofluid, stability is maintained by electrostatic and repulsive interactions between counterions and amphoteric hydroxyl ions ($H_3O^+$ or $OH^-$). TEOS solution was added and reacted with $H_2O$ adsorbed on the surface of $Fe_3O_4$ to connect Si–O with nanoparticles. Further hydrolysis of TEOS causes $-OCH_2CH_3$ to transfer into –OH. The adjacent –OH group loses a molecule of $H_2O$ to form a cross-linked structure and subsequently $SiO_2$ coating is formed. $Fe_3O_4/SiO_2$ nanocomposites prepared in this manner can resist corrosion of strong acid or base, indicating that $Fe_3O_4$ nanoparticles are capsulated by $SiO_2$.

## 4. Conclusions

Spherical $Fe_3O_4/SiO_2$ nanocomposites were synthesized by a two-step process. First, magnetic nanoparticles were dispersed in aqueous solution in the presence of TMAOH. Then silica shell was formed on $Fe_3O_4$ nanoparticles from the hydrolysis of TEOS catalyzed by $OH^-$ adsorbed on the surface of magnetic nanoparticles. Characters of the nanocomposites such as magnetism, morphology and stability were studied. The saturation of magnetization decreased with reduced amount of $Fe_3O_4$, but maintained superparamagnetism. The nanocomposites are stable in dilute acidic or basic solution and at high temperature. Bioconjugation ability was tested by connecting $SiO_2/Fe_3O_4$ nanocomposites to antibody.

**Acknowledgements** This work was funded by High-Technology Research and Development Program of China (No. 2003BA310A28), National Natural Science Foundation of China (No. 10574047) and Doctor Foundation of China (No. 20030487003).

## References

1. Kobayashi Y, Horie M, Konno M, Rodrıǵuez-Gonzaléz B, Liz-Marzań LM (2003) J Phys Chem B 107:7420
2. Mikhaylova M, Kim D, Bobrysheva N, Osmolowsky M, Semenov V, Tsakalakos T, Muhammed M (2004) Langmuir 20:2472
3. Kim DK, Mikhaylova M, Wang FH, Kehr J, Bjelke B, Zhang Y, Tsakalakos T, Muhammed M (2003) Chem Mater 15:4343
4. Liu ZL, Liu YJ, Yao KL et al (2002) J Mater Synth Proces 10:83
5. Liu ZL, Wang X, Du GH, Lu QH, Ding ZH, Tao J et al (2004) J Mater Sci 39:2633
6. Liu ZL, Wang HB, Lu QH, Du GH, Peng L, Du YQ, Zhang SM, Yao KL (2004) J Magn Magn Mater 283:258
7. Gruttner C, Teller J (1999) J Magn Magn Mater 194:8
8. Tartaj P, Gonzaléz-Carren T, Serna CJ (2003) J Phys Chem B 107:20
9. Liu ZL, Ding ZH, Yao KL, Tao J, Du GH, Lu QH, Wang X, Gong FL Chen X (2003) J Magn Magn Mater 265:98
10. Corrias A, Casula MF, Ennas G, Marras S, Navarra G, Mountjoy G (2003) J Phys Chem B 107:3030
11. Casas L, Roig A, Rodríguez E, Molins E, Tejada J, Sort J (2001) J Non-cryl Sol 285:37
12. Grasset F, Labhsetwar N, Li D, Park DC, Saito N, Haneda H, Cador O, Roisnel T, Mornet S, Duguet E, Portier J (2002) J Etourneau Langmuir 18:8209
13. Vestal CR, Zhang ZJ (2003) Nano Lett 3:1739
14. Graf C, Vossen DLJ, Imhof A (2003) A van Blaaderen Langmuir 19:6693
15. Ohmori M, Matijevic E (1993) J Colloid Interface Sci 160:288
16. Ohmori M, Matijevic E (1992) J Colloid Interface Sci 150:594
17. Lian SY, Kang ZH, Wang EB, Jiang M, Hu CW, Xu L (2003) Solid State Commun. 127:605